

# Towards a Top / Anti-top Cross Section Measurement at ATLAS using High $P_T$ $e\mu$ Events

John Phillips  
Duke University  
Dept. of Physics

The goal of this analysis is to produce a system of cuts to isolate the top / anti-top production signal against backgrounds. The  $e\mu$  decay mode was used. The primary backgrounds considered were  $WW$  and  $Z \rightarrow \tau\tau$ . The secondary backgrounds considered were the class of backgrounds where a jet is misreconstructed as a lepton. Among this class of backgrounds,  $Wbb$  was chosen as a representative process. Using the standard top group Monte Carlos produced at 10 TeV, the kinematics of particle collisions were studied and various cuts were derived to improve the ratio of signal to background. This system of cuts was effective at suppressing the primary backgrounds, however more study will be needed to effectively reduce the  $W + \text{jets}$  class of backgrounds.

# **Acknowledgments**

I am grateful to the Duke University Physics Department. Without their support this thesis could not have been completed. In particular, I would like to thank Dr. Mark Kruse for the guidance he provided as my faculty mentor during this process.

# The Standard Model

The Standard Model describes our current knowledge about the physics of fundamental particles. All particles can be divided into two classes: fermions possessing half-integer spin and bosons possessing integer spin. The Standard Model accounts for four fundamental bosons, each of which is associated with a fundamental force. Fermions are divided into two groups: those that are subject to the strong nuclear force, called quarks; and those that aren't, called leptons. There are six quark types and six lepton types. Fermions also have anti-particles, which have identical masses, but opposite quantum numbers to their conjugates.

## Force Mediators

Each of the fundamental forces is mediated by the exchange of a boson. The bosons associated with the forces described by the Standard Model are all spin-1. The proposed graviton, mediator of the gravitational force, is spin-2, however it has yet to be observed, and gravity is not easily incorporated into the Standard Model. Table 1 lists some properties of the force mediating bosons.

	Associated Force	Relative Strength	Electrical Charge	Mass (GeV)
gluon (g)	Strong	1	0	0
photon ( $\gamma$ )	Electromagnetic	$10^{-3}$	0	0
Z	Weak	$10^{-14}$	0	92
W			$\pm 1$	80

Table 1 – Properties of Force Mediating Bosons [1][2]

## Leptons

There are six leptons divided into three generations. Leptons from the same generation share the same lepton quantum number, which is conserved in particle interactions. Within each generation, one lepton carries an electrical charge and one does not. The neutral particle is called a neutrino. Table 2 gives some properties of leptons.

		Electrical Charge	Quantum Number	Mass (GeV)
First Generation	electron (e)	-1	$L_e = 1$	$0.511 \times 10^{-3}$
	$\nu$	0	$L_e = 1$	$< 2 \times 10^{-9}$
Second Generation	muon ( $\mu$ )	-1	$L_\mu = 1$	0.1
	$\nu_\mu$	0	$L_\mu = 1$	$< 2.0 \times 10^{-4}$
Third Generation	tau ( $\tau$ )	-1	$L_\tau = 1$	1.78
	$\nu_\tau$	0	$L_\tau = 1$	$< 1.8 \times 10^{-2}$

Table 2 – Properties of Leptons. [1]

## Quarks

The six types of quarks fall into three generations: down and up (First Generation), strange and charm (Second Generation), bottom and top (Third Generation). All quarks bear non-integer electrical charge: each generation has one quark bearing  $+2/3$  electrical charge (up, charm, top), and one with  $-1/3$  (down, strange, bottom).

The defining feature of quarks is that they are subject to the strong nuclear force. Quarks carry color charge; a quark can be red, blue, or green, while an anti-quark can be anti-red, anti-blue, or anti-green. These labels have nothing to do with everyday notions of color; rather, they are labels devised to convey the three dimensional nature of charges associated with the strong force (as opposed to the electromagnetic charge, which comes in two varieties: positive and negative). Observable particles are colorless; therefore, we do not expect to be able to observe an isolated quark. Quarks are always found in bound states, called hadrons. Baryons are hadrons composed three quarks or three anti-quarks, each carrying a different color charge. For instance, a proton has two up quarks and a down quark. Mesons are composed of a quark and an anti-quark bearing conjugate color charges. For example, a charged pion,  $\pi^+$  or  $\pi^-$ , has an up and an anti-down and a down and an anti-up, respectively.

Table 3 lists some properties of quarks.

		Electrical Charge	Quantum Number	Mass (GeV)
First Generation	up	+2/3	U = 1	$2 \times 10^{-3}$
	down	-1/3	D = -1	$5 \times 10^{-3}$
Second Generation	charm	+2/3	C = 1	1.2
	strange	-1/3	S = -1	0.10
Third Generation	top	+2/3	T = 1	174
	bottom	-1/3	B = -1	4.20

Table 3 – Properties of quarks. [1]

## The Top Quark

The top quark seems to be an interesting particle. Its mass is almost two orders of magnitude greater than any other quark. Furthering our understanding of the top quark could help us unlock new physics. The ultimate goal of this analysis is to produce a simple set of cuts to isolate top quark events that can be used for analyses to measure top quark properties.

# The LHC and ATLAS

This section contains discussion on the Large Hadron Collider (LHC) and A Toroidal LHC ApparatuS (ATLAS). The (LHC) is located at the European Organization for Nuclear Research (CERN) on the France-Switzerland border near Geneva, Switzerland. The LHC is capable of accelerating protons to 7 TeV, making possible the highest energy collisions in the world. The largest detector at CERN, ATLAS represents a collaboration of 169 institutions in 39 countries. It is dedicated to the search for new physics; in particular, scientists at ATLAS are interested in observing the Higgs boson, which is responsible for giving fundamental particles mass.

## The LHC Accelerator system

Protons to be used at one of the LHC's six experiments are formed by stripping the electron from atomic hydrogen. The protons then pass through the linear accelerator, through the Proton Synchrotron Booster, and into the Proton Synchrotron (PS). The PS was CERN's first synchrotron, and accelerates protons to 25 GeV. From the PS, the protons are transferred to the Super Proton Synchrotron (SPS), a ring 7 km in circumference. The SPS accelerates the protons to 450 GeV. Finally, the protons reach the LHC ring, where after about 20 minutes, they reach their maximum velocity [4].

## The LHC Ring

The LHC ring is 27 km in circumference and 100 m underground. Figure 1 is a schematic of the LHC ring. Proton bunches travel in opposite directions around the ring in parallel beam pipes. Each beam has a design energy of 7 TeV, corresponding collisions at 14 TeV center-of-mass energy. This energy corresponds to the temperature of the universe when it was  $10^{-14}$  seconds old [6]. As of now, the LHC is running at 3.5 TeV per beam. The beams are composed of roughly cylindrical bunches of about a billion protons with radii on the order of nanometers. Each bunch is separated by about 7.5 meters. Since the protons are traveling very close to the speed of light, bunches collide every 25 ns, or at a frequency of 40 million Hz. Each time a bunch collides, around 20 collisions occur when running at design luminosity.

To bend the beams around the ring, the LHC ring has 1232 dipole magnets, each 15 m in length. These magnets operate in a superconducting state. Superconducting materials, when held at very low temperatures, are capable of conducting electricity with minimal energy loss due to resistance. To keep temperatures low, the magnets are cooled to 2 K with liquid helium. In addition to the dipole magnets 392 quadrupole magnets focus the beam. The beams can be made to collide at any of four collision points, corresponding to the locations of the LHC detectors: ATLAS, A Large Ion Collider Experiment (ALICE), the Compact Muon Solenoid (CMS), and Large Hadron Collider beauty detector (LHCb). Two additional experiments study 'forward particles,' particles that brush past each other rather than colliding head on. These experiments are located near the larger detectors:

TOTAL Elastic and diffractive cross section Measurement (TOTEM), located near CMS; and Large Hadron Collider forward (LHCf), located near ATLAS [4].

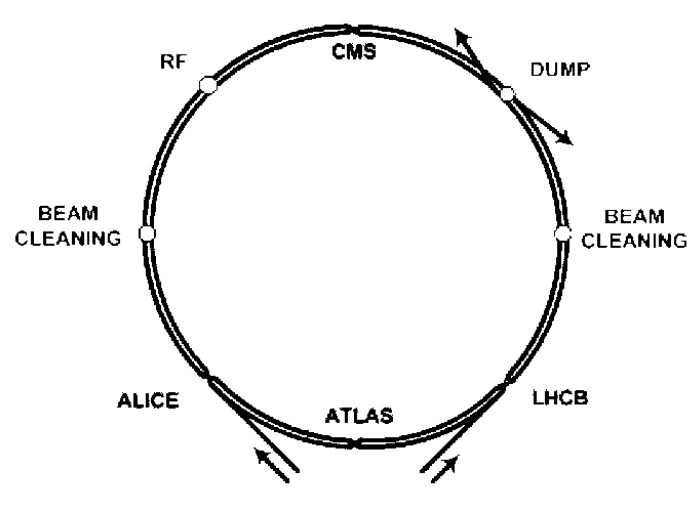


Figure 1 – Diagram of LHC ring. [6]

## ATLAS Detector

The ATLAS detector is an all-purpose CERN detector. At 7000 tons, ATLAS is the largest particle detector in the world. The detector has three main sections: the inner detector, which measures the momentum of charged particles; the calorimeter, which measures the energy of electrons, photons, and quarks; and the muon spectrometer, which measures the momentum of muons.

### The Inner Detector

The inner detector is designed to measure the momentum of charged particles. The inner detector is surrounded by a solenoid that generates a 2 T magnetic field. The charged particles bend in the magnetic field, allowing us to measure their momentum. There are three components to the inner detector: the pixel detector, the silicon strip detector, and the transition radiation detector. Figure 2 is an illustration of the inner detector.

The pixel detector is composed of 140 million silicon pixels, each 50 by 300 microns in dimension. Each time a charged particle passes through a pixel, a signal is recorded. The first layer of pixels is located 50.5 mm from the center of beam pipe. This allows for extremely precise measurement of particle positions and trajectories, precise enough to determine if the particle originated from the collision point, or from the decay of a particle produced at the collision point (for example a b quark will typically travel a few mm before decaying).

The second layer of the inner detector is the Silicon Central Tracker (SCT). Rather than silicon pixels, this layer is composed of silicon strips 80 microns wide and centimeters long. Like the pixel detector, the silicon produces a signal when a charged particle passes

through it. The strip detectors are less precise than the pixel detectors, however they are more cost effective.

The outer layer of the inner detector is the Transition Radiation Tracker (TRT). This layer is composed of 370,000 straw drift tubes 4 mm in diameter placed in 60 layers. The straws are filled with Xenon gas. When a charged particle passes through the straw, the Xenon is ionized, and a signal travels along the wire in the center of the straw. By timing the signals produced, the impact parameter can be determined. Along the barrel, the straws run parallel to the beam pipe; in the TRT endcaps, the straws run radially [5]. The ATLAS group at Duke played a major role in the design and construction of the TRT.

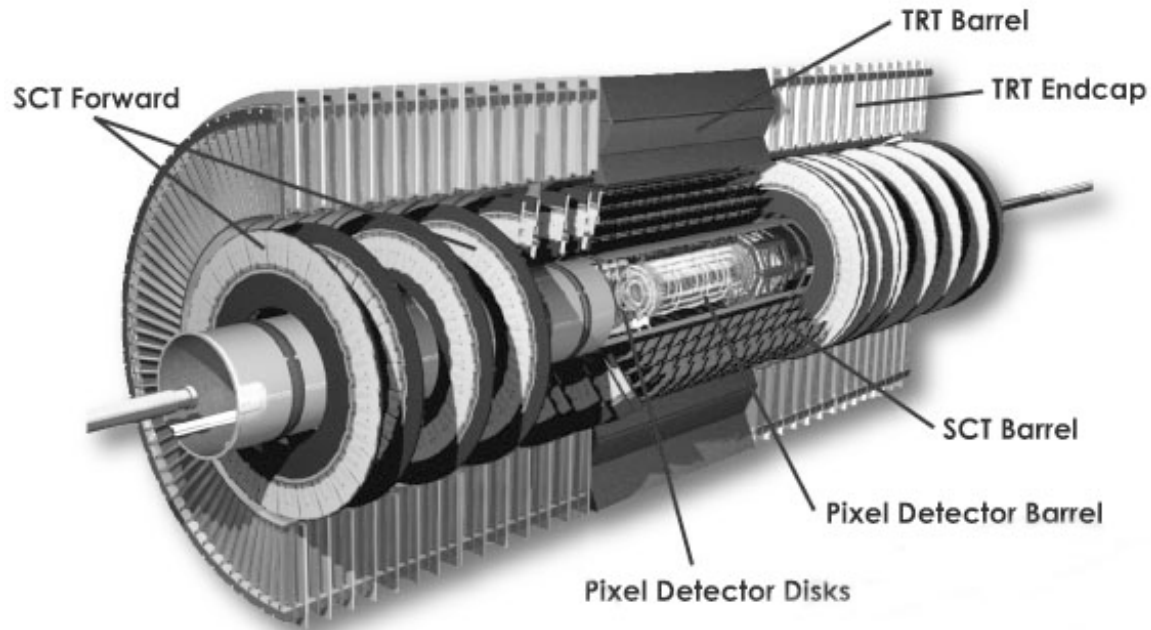


Figure 2 – Schematic of the Inner Detector [5].

## The Calorimeter

The middle layer of the ATLAS detector is the calorimeter. There are two components to the calorimeter: the Electromagnetic Calorimeter and the Hadron Calorimeter. The electromagnetic calorimeter consists of lead plates immersed in a bath of liquid argon. When photons or electrons encounter the lead, they produce a shower of low-energy electrons and positrons. The number of electrons and positrons in the shower is proportional to the energy of the incident particle. The shower of electrons encounters the argon, which is in an electric field. The electrons from the shower ionize the argon, and the ionized electrons are carried by the electric field, creating a signal. Thus the amount of current in the signal is related to the energy of the incident particle. The calorimeter electrodes are grouped together into towers, which determine the direction in which the energy is deposited. This assists in the identification of jets.

The Hadronic Calorimeter is composed of metal plates separated by scintillating plastic. When hadrons hit the metal plates, they produce a shower of particles, called a ‘hadronic

shower,' composed of low energy hadrons. The hadronic shower interacts with the plastic to produce photons, which are converted into a signal. The barrel portion of the calorimeter uses iron to produce the showers, while the endcap calorimeter uses copper, and uses liquid argon as the scintillating material. Jets deposit their energy in both the Electromagnetic Calorimeter and the Hadronic Calorimeter, so these measurements must be combined to get the full jet energy. Photons and electrons are stopped by the Electromagnetic Calorimeter and do not make it to the Hadronic Calorimeter.

## The Muon Chamber

The only charged particles that can make it through the calorimeters are muons. The outer portion of the ATLAS detector is dedicated to the measurement of muon trajectories. The muons are subject to magnetic fields produced by toroidal magnets so that their trajectories are deflected either towards or away from the beam pipe. The primary devices used to measure muon trajectories are monitored drift tubes. These 3-cm diameter glass-field tubes operate in a similar manner to the TRT. A muon passing through the tube produces a signal, and by observing the timing of the signals, we can determine the impact parameter of the passing muon. By matching up the track in the muon detector with a track from the inner detector, we can determine the trajectory of the muon. The only particles that make it through the muon detectors undetected are the neutrinos, which rarely interact with matter, and whose presence can only be inferred by missing energy (this will be discussed in more detail later) [5].

Figure 2 illustrates the behavior of particles in the various sections of the ATLAS detector. Notice that the neutral photons and neutrons do not react with the inner detector.

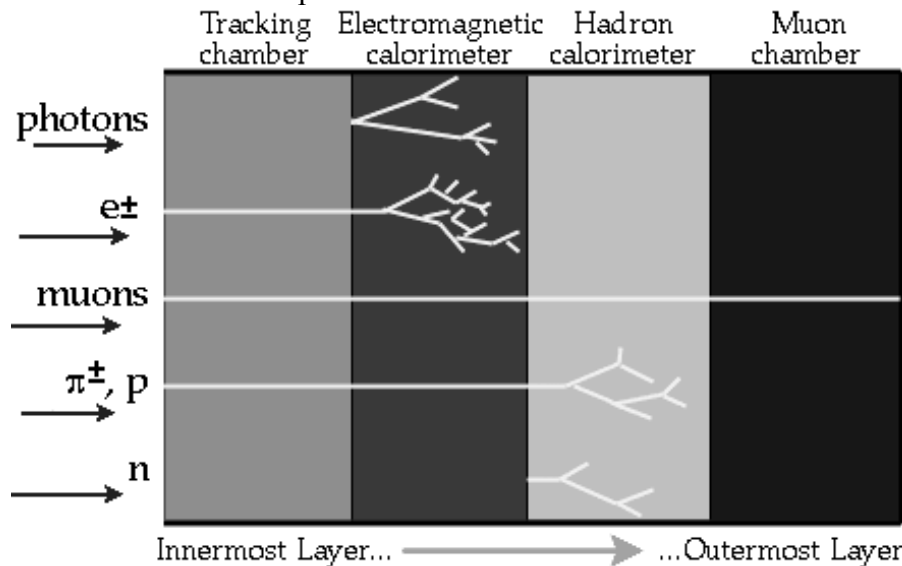


Figure 2 – Interactions of various particles with the ATLAS detector[5]

# Discussion of Standard Model Processes

This section contains discussion about the three primary Standard Model processes contained in this analysis: our signal, t-tbar\* production; and our primary backgrounds, WW production and  $Z \rightarrow \tau\tau$  (the Drell-Yan process). We will also briefly discuss secondary backgrounds arising from a jet being misinterpreted as an electron. We will treat Wbb as a representative process of this class of background. This analysis uses Monte Carlo data generated at 10 TeV, so all cross sections listed are given at this energy.

## Signal Process – ttbar production

For this analysis, we will consider t-tbar production to be our signal process. At LHC energies, the primary mechanism by which a t-tbar pair is produced is gluon-gluon fusion:  $gg \rightarrow t\text{-tbar}$ . At lower energies, such as at the Tevatron, production of t-tbar pairs via quark annihilation dominates:  $q\text{-qbar} \rightarrow t\text{-tbar}$ . The cross-section for this process is 414 pb at the LHC.

Upon production, the t quickly decays into a W boson and a b. From there, the W can decay in one of several ways. Because of this, we must consider the branching ratio of each decay mode. Each W can decay either hadronically:  $W^+ \rightarrow (u\text{-dbar})(c\text{-sbar})$ ,  $W^- \rightarrow (d\text{-ubar})(s\text{-cbar})$ ; or leptonically:  $W^\pm \rightarrow (e^\pm \nu)(\mu^\pm \nu)(\tau^\pm \nu)$ . Thus there are three decay channels: all-hadronic, lepton + jets, and dilepton. Hadronic decay is characterized by an additional degree of freedom associated with the color charge. The W boson is colorless and can decay into three possible color combinations: (red, anti-red)(green, anti-green)(blue, anti-blue). We are now able to compute the branching ratios for the various t-tbar decay modes, which are given in Table 4.

Decay Channel	Decay Mode	Branching Ratio	
Dilepton	$e\nu b e \nu b$	1/81	9/81 (11%)
	$\mu\nu b \mu\nu b$	1/81	
	$e\nu b \mu\nu b$	2/81	
	$e\nu b \tau\nu b$	2/81	
	$\mu\nu b \tau\nu b$	2/81	
	$\tau\nu b \tau\nu b$	1/81	
Lepton + Jets	$qq b e \nu b$	12/81	36/81 (44%)
	$qq b \mu\nu b$	12/81	
	$qq b \tau\nu b$	12/81	
All-Hadronic	$qq b qq b$	36/81	36/81 (44%)

Table 4 – Branching ratios for t-tbar decay modes [3].

\*for this analysis, the suffix -bar refers to a particle's conjugate, e.g. tbar refers to anti-top

Highlighted in the above table is the  $e\mu$  decay mode, which is the one we will be considering in this analysis. This decay channel is fairly well separated from the background, motivating the selection of a decay mode with a low branching ratio. Note that we require that the electron and the muon be oppositely charged. Figure 3 gives the leading order Feynman diagram for the overall process we will be considering:  $gg \rightarrow t\text{-}t\text{bar} \rightarrow e\nu b\mu\nu b$ .

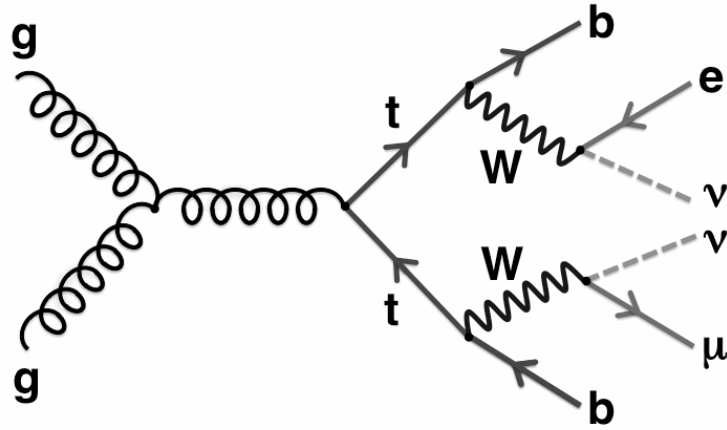


Figure 3 – Leading order Feynman diagram for t-tbar production and dileptonic decay.

### Main Background Processes – WW

One of our primary backgrounds is WW production and decay, the leading order Feynman diagram for which is given in Figure 4. Charge conservation requires that the parent W bosons be oppositely charged, implying the daughter leptons would also carry opposite charge. The decay modes for this process are identical to those given above, except that the event contains no b quarks. As a result, we would once again expect the branching ratio for the  $e\mu$  mode to be  $2/81$ . The WW cross section is 74 pb.

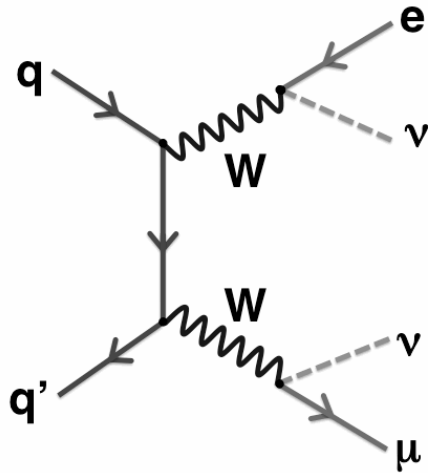


Figure 4 – Leading order Feynman diagram for WW production and dileptonic decay.

### **Z→ττ (Drell-Yan Process)**

The other primary background we will concern ourselves with is Z boson decay. The branching ratio for the ττ decay of the Z boson is approximately 3.37%. Each τ then may undergo the process  $\tau^\pm \rightarrow e^\pm \nu_e \nu_\tau$  or  $\tau^\pm \rightarrow \mu^\pm \nu_\mu \nu_\tau$ . The branching ratio for eμ production is about 6%, meaning that the overall branching ratio for  $Z \rightarrow \tau\tau \rightarrow e\nu\mu\nu\nu$  is 0.21%. In spite of this small branching ratio, we still expect this process to constitute a substantial background as its cross section is high relative to the other processes being considered. Here again, charge conservation implies that the final lepton products will bear opposite charge. The leading order Feynman diagram for this process is given in Figure 5. The  $Z \rightarrow \tau\tau$  cross section is 1210 pb.

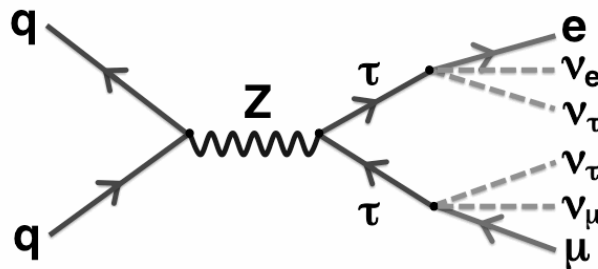


Figure 5 – Leading order Feynman diagram for the Drell-Yan process.

## Secondary Background Processes

Our secondary backgrounds consist of processes where a real muon is produced and a non-electron passes the electron selection criteria and is misidentified as an electron. The process we will consider is  $Wb\text{-}b\bar{b}$  (for conciseness, we'll call this  $Wbb$ ), where one of the  $b$  jets is misidentified as an electron. Jets and electrons deposit significant amounts of energy into the calorimeter, which motivates considering these processes as substantial backgrounds.

# Particle Identification

This section includes discussion on the tracking and identification of particles. We must first establish the geometry of the detector and define terms that will be used to describe event parameters. Discussion of the identification of leptons, jets, and neutrinos follows.

## Detector Geometry

In order to accurately describe the kinematics of the collision, we will impose a cylindrical coordinate system on the detector, where the  $z$  direction is along the beam axis. The azimuthal angle -  $\phi$  - is defined as the angle a vector makes in a plane perpendicular to the beam axis, relative to the  $x$ -axis which points radially outwards from the center of the LHC. The plane in which these vectors lie is called the 'transverse plane,' defined by the  $x$  and  $y$  axes. The physical significance of the transverse plane is tied to momentum conservation: each component of momentum must be conserved in the collision. There is substantial uncertainty associated with the  $z$  component of momentum, arising from non-equal energies of colliding quarks and gluons. However, since both particles are traveling entirely in the  $z$  direction, the transverse component of momentum for the overall collision is in principle zero. This property of the transverse plane makes transverse-component measurements extremely useful, particularly for the indirect detection of neutrinos.

It is conventional to express distances in the  $z$  direction in terms of *pseudorapidity* ( $\eta$ ). The rapidity of a particle is given by:

$$Y = \frac{1}{2} \ln[(E+p_z)/(E-p_z)]$$

For highly relativistic particles, where the mass term is small compared to the total energy, this reduces to

$$\eta = -\ln[\tan(\theta/2)]$$

where  $\theta$  is the usual polar angle measured from the interaction point at  $z_0$ . For trajectories perpendicular to the beam, that is, entirely in the transverse plane,  $\eta = 0$ . Also, we have the properties

$$\eta[\pi/2+\theta] = -\eta[\pi/2-\theta]$$

$\eta$  is infinite at  $\theta = 0, \pi$  (i.e. along the beam axis).

The angle associated with  $\eta = 0$  is  $90^\circ$ ,  $\eta = 1$  is  $40.4^\circ$ ,  $\eta = 2$  is  $15^\circ$ ,  $\eta = 3$  is  $5.70^\circ$ ,  $\eta = 4$  is  $2.10^\circ$ .

## Lepton Identification

Electrons are charged, so they create a track through the inner detector, and deposit their energy entirely in the EM calorimeter. By matching its track to a shower in the calorimeter, the electron can be tagged. Additional kinematic constraints are applied to the electron candidates in order to accept real electrons and reject background events. In particular, for this analysis, we require a “good” electron (a Cuteuple tag that selects electron candidate events based on parameters such as shower profile, track isolation, and track to calorimeter matching) with  $P_T > 20$  GeV.

Muons are minimally ionizing particles, so while they may lose some energy in the calorimeter, they are not stopped by it. Muon selection is primarily based on matching a track in the inner detector to a track in the outer detector. Once again, this analysis requires a “good” muon with  $P_T > 20$  GeV.

## Jet Identification

A hadronizing quark creates a shower of particles in the detector called a jet. This quark fragmentation is a result of color confinement: as the oppositely color-charged quarks separate, it becomes more energetically favorable for a quark / anti-quark pair to fall out of the vacuum than for the distance between the original quarks to continue to increase. Jets deposit energy in both the EM and hadronic calorimeters. The tower arrangement of calorimeter electrodes allows the four-momentum of the jets to be determined [e\_tour]. This analysis rejects all jet candidates with  $P_t < 25$  GeV. Additionally, because electrons are often misidentified as jets, we impose the additional requirement  $\Delta R_{\text{lepton,jet}} > 0.4$ , where

$$\Delta R \equiv [(\Delta\phi)^2 + (\Delta\eta)^2]^{1/2}$$

## Neutrino Detection

Neutrinos bear neither color charge nor electrical charge, so they rarely interact with matter, as they can only experience the weak interaction. Because of this, we can not detect them directly; however, we can use conservation of momentum to infer their presence. The vector sum of the transverse momentum of the system must equal zero. Note that special relativity gives the result:

$$E = p$$

establishing the equivalence of momentum and energy for highly relativistic particles where the mass term can be neglected. Therefore, we need draw no distinction between the conservation of vector momentum and scalar energy. The equation for determining the energy associated with neutrinos (the “missing transverse energy” which we’ll call MET) is nominally

$$\text{MET} = -\sum E_{T, \text{ calorimeter}} - \sum P_{T \text{ muons}}$$

where  $\sum E_{\text{calorimeter}, \eta=0}$  is the energy deposited in the calorimeter in an annulus around the interaction point. However, additional corrections must be imposed due to the muons depositing a small amount of energy in the calorimeter, and due to any additional energy loss due to uninstrumented regions in the detector.

# Collision Kinematic Analysis

The goal of this analysis is to devise a system of cuts to improve the signal to background ratio for  $t$ - $\bar{t}$  against various backgrounds, namely  $WW$ ,  $Z \rightarrow \tau\tau$ , and  $Wbb$ . The latter process is taken as a representative member of the class of background processes  $W$  + jets, where one of the jets ‘fakes’ an electron signal. To that end, we will examine the dynamics of 10 TeV Monte Carlo (MC) collision data. The MC samples used are the standard top group MCs. The ‘‘CuteTuple’’ Ntuple format was used, a data format developed by Dr. Ayana Arce.

## Lepton Kinematics

The electron  $P_T$  spectra for the processes being considered are given in Figure 6. Figure 7 gives their respective muon  $P_T$  spectra. The hard cut-off at 20 GeV is an artifact of the  $P_T$  requirement placed on the accepted electron candidates.

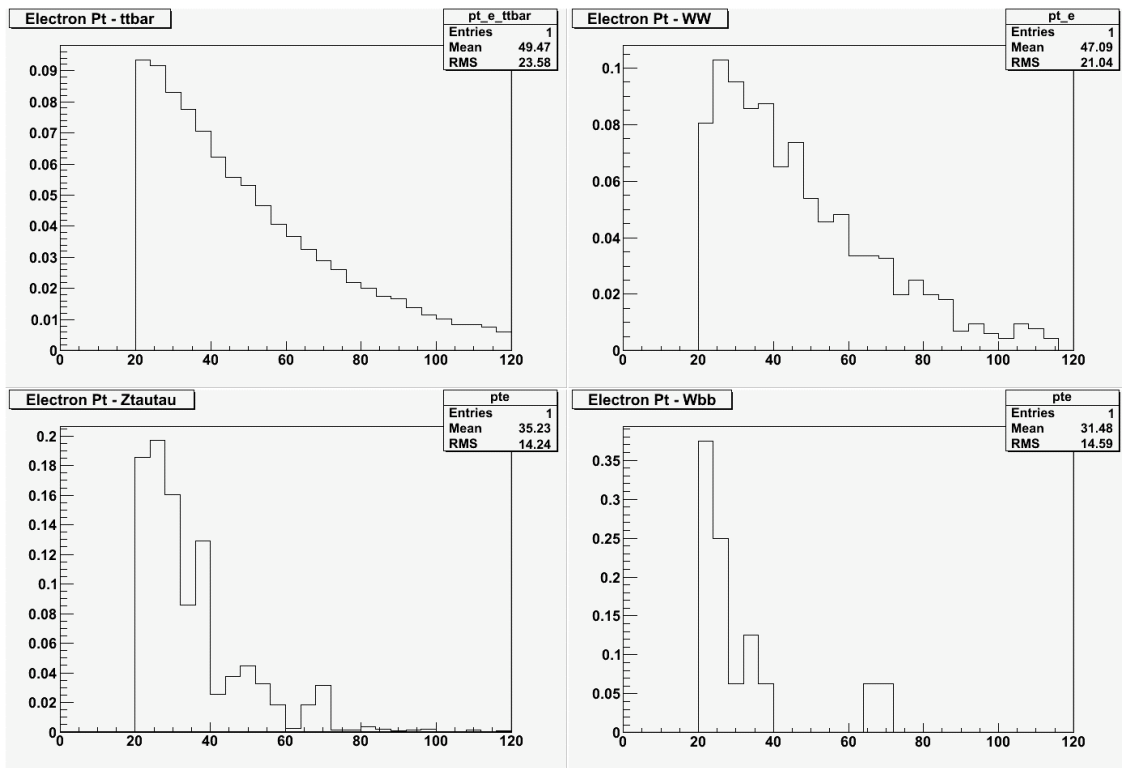


Figure 6 – Electron  $P_T$  distributions.

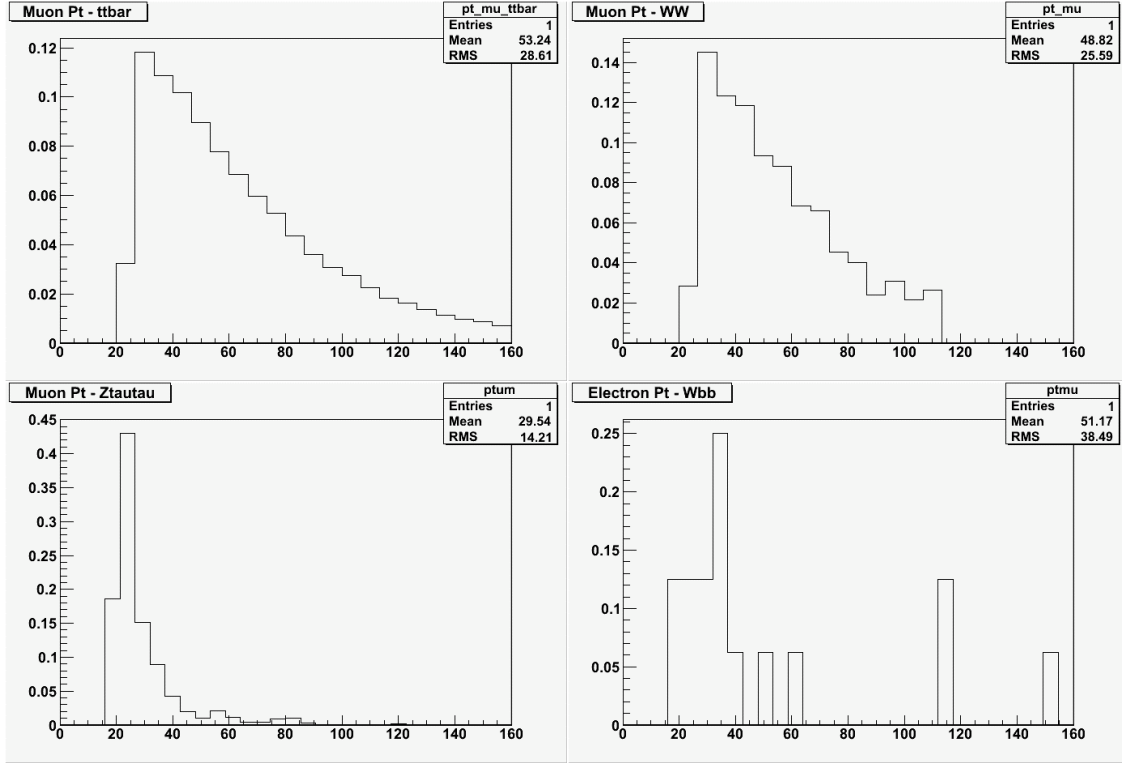


Figure 7 – Muon  $P_T$  distributions.

Note the similarities between the  $t$ - $\bar{t}$  and  $WW$  distributions and the  $Z \rightarrow \tau\tau$  and  $Wbb$  distributions. The former group has substantially more high  $P_T$  electrons, because both leptons in these events come from the decay of a  $W$  boson. The latter distributions are skewed towards lower  $P_T$  values. In the case of  $Z \rightarrow \tau\tau$ , the leptons come from further decay of the  $\tau$ . For  $Wbb$ , one jet must come from a  $b$  jet faking a lepton signature, and the  $b$  jet energy spectrum is steeply falling.

The distributions appear to peak at lower momentum values than conservation of energy would require. For instance, we would expect the  $t$ - $\bar{t}$  electron spectrum to peak near 40 GeV, while the above plot peaks at  $< 20$  GeV. However, this is a result of only a component of the total electron energy being reported. Figure 8 shows the electron energy distribution, and we can see that it peaks higher as expected due the additional energy component in the  $z$  direction. Figure 9 is the  $\eta$  distribution for the events. The events with greater  $|\eta|$  have a lower component of momentum in the transverse plane.

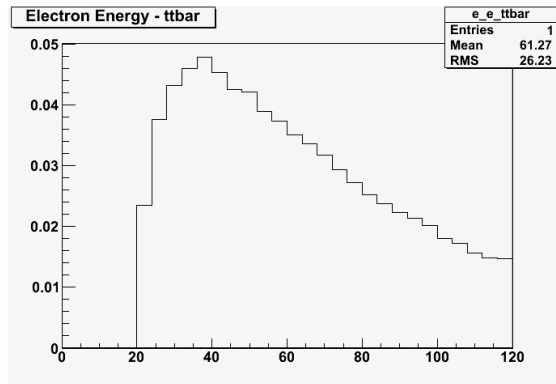


Figure 8 – Electron energy distribution.

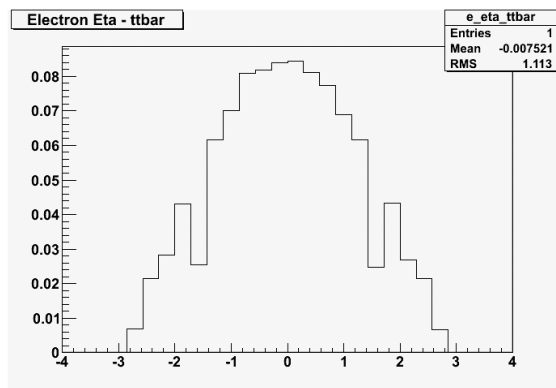


Figure 9 – Electron pseudorapidity spectrum.

## Missing Transverse Energy

Figure 10 gives the MET spectra for the four processes.

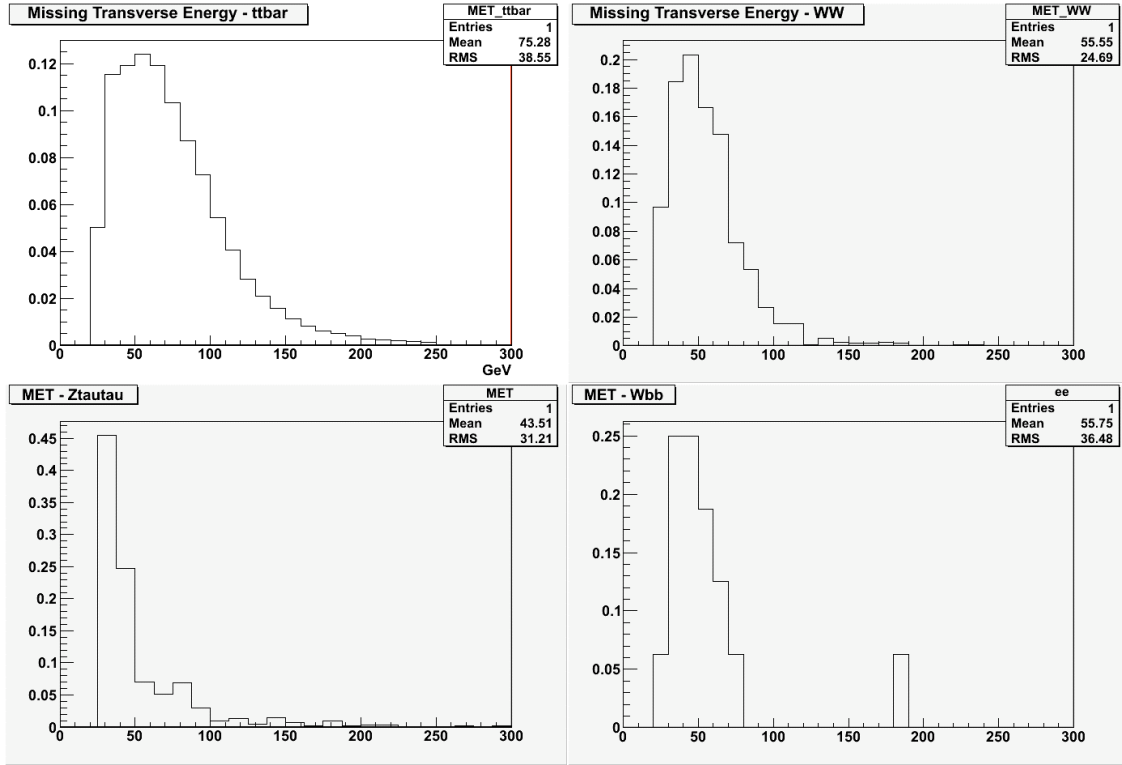


Figure 10 – Missing Energy Distribution.

As is the case with leptons, we observe a greater number of high MET events in the distributions of  $t\text{-}\bar{t}$  and WW than  $Z\rightarrow\tau\tau$  and Wbb. This is, again, because the neutrinos in the  $t\text{-}\bar{t}$  and WW events come from the decay of a W boson, while the neutrinos in  $Z\rightarrow\tau\tau$  come from the further decay of a  $\tau$ . Additionally, neutrinos in this process tend to be directed in opposite directions, decreasing their vector sum. Wbb contains only one W decaying leptonically, as opposed to two in  $t\text{-}\bar{t}$  and WW, so we would also expect that distribution to skew towards lower MET values.

## Jet Multiplicity

The jet multiplicity distributions are given in Figure 11.

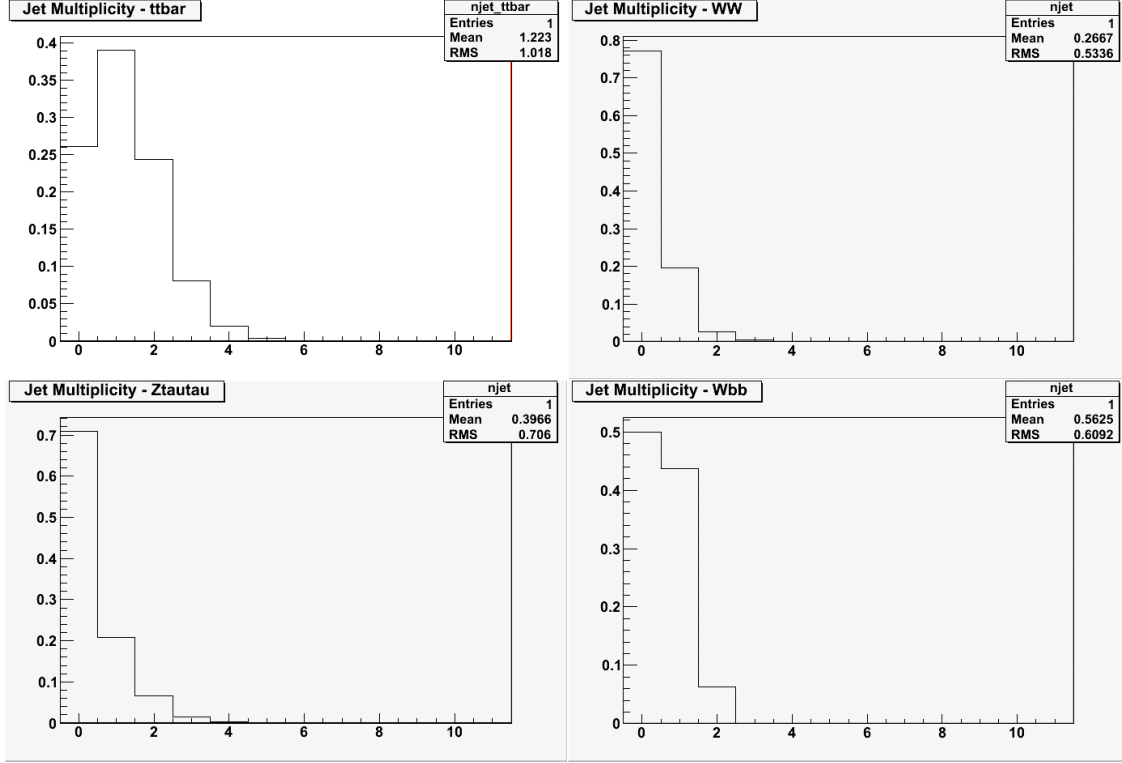


Figure 11 – Jet multiplicity distributions.

As expected, the WW and  $Z \rightarrow \tau\tau$  distributions peak strongly at  $n_{\text{jets}} = 0$ . These processes do not contain any jets in their lowest order Feynman diagrams; the jets we observe are a result of contributions from higher order corrections.

The t-tbar and Wbb jets are a bit more surprising. In principle, we might expect both events to peak strongly at  $n_{\text{jets}} = 2$ , since both processes contain two jets at lowest order. However, t-tbar peaks at  $n_{\text{jets}} = 1$  and Wbb peaks at  $n_{\text{jets}} = 0$ . In the case of t-tbar, this can likely be explained by the  $P_{\text{T}}$  requirement placed on the jets. Although the jet energy peaks substantially above the 25 GeV cut imposed on the jet candidates, it is possible that many jets are detected at a high enough  $\eta$  that transverse component of their momentum falls below the cut. Further study of the kinematics of jet production in t-tbar production might be required to understand why the distribution does not peak where one might expect it to.

In the case of Wbb, there is an additional subtlety to the distribution. The lowest order Feynman diagram for this process contains two jets, so one might naively expect the distribution to peak at  $n_{\text{jets}} = 2$ . However, we are only considering events where one of the jets is counted as a lepton. If a jet passes the electron selection criteria, it will be doubly counted as both an electron and a jet. We apply an overlap-removal cut to the jet candidates, rejecting them if a lepton is found within  $\Delta R = 0.4$ . Therefore all events plotted above contain at least one jet that failed the overlap-removal cut.

## Angular Separation between MET and Leptons

Figure 12 gives the angular separation between the MET (in vector form) and the nearest lepton track, projected onto the transverse plane ( $\Delta\phi$ ).

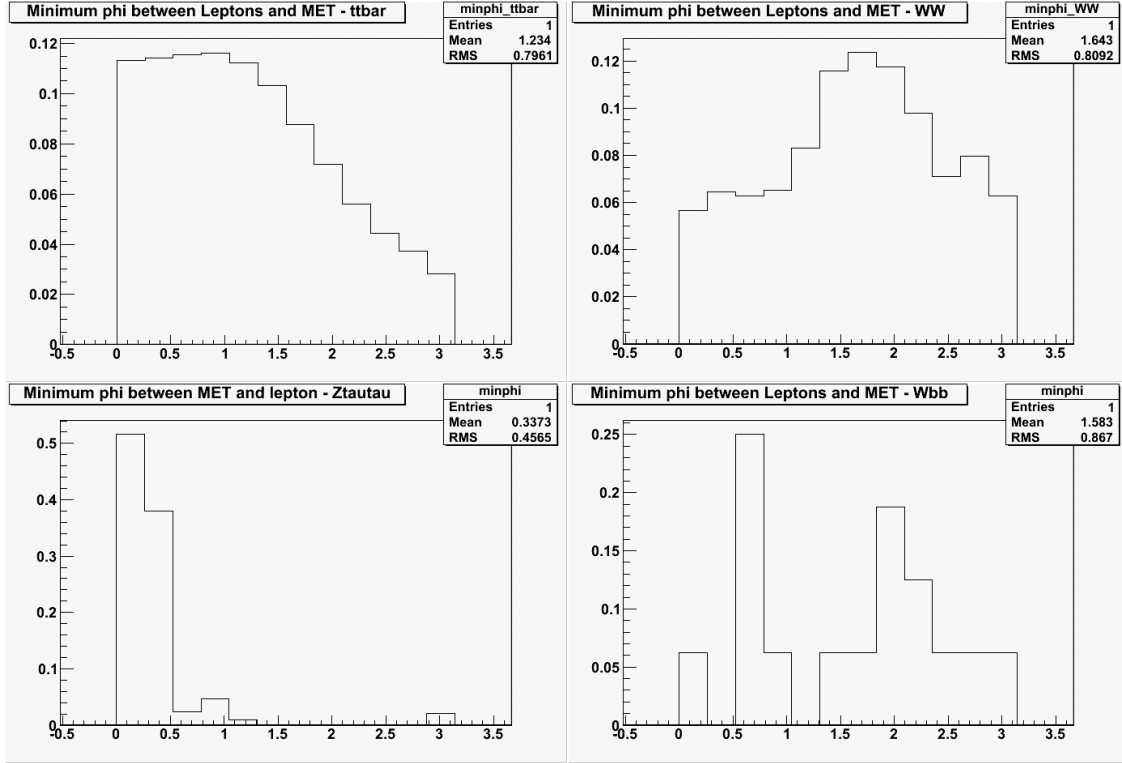


Figure 12 -  $\Delta\phi$  between MET and nearest lepton.

The t-tbar appears flat in the low  $\Delta\phi$  domain, and slope gradually downward as  $\Delta\phi$  approaches  $\pi$ . The WW distribution appears to peak at  $\pi/2$ . We can draw no conclusions as to the Wbb  $\Delta\phi$  distribution.

The  $Z \rightarrow \tau\tau$  distribution is very strongly peaked near  $\Delta\phi = 0$ . The physical explanation for this is that the observed leptons come from the decay of  $\tau$  leptons. The  $\tau$  are much more massive than the electrons, muons, or neutrinos, so to conserve momentum, the daughter particles must emerge highly collinear to the track of the parent  $\tau$ .

## Partons

It is instructive to consider the effect of higher order Feynman diagrams than those given in Section 3. The above plots were made with high order terms considered, however we wish to address their kinematics independently. These higher order corrections come from additional gluons radiated by the particles, called partons. To this end, we will plot

the above kinematic parameters of  $Z \rightarrow \tau\tau$  for each number of partons from 0 to 5. Figure 13 is electron  $P_T$ , Figure 14 is muon  $P_T$ , Figure 15 is MET, Figure 16 is jet multiplicity, Figure 17 is  $\Delta\phi$  between MET and the nearest lepton.

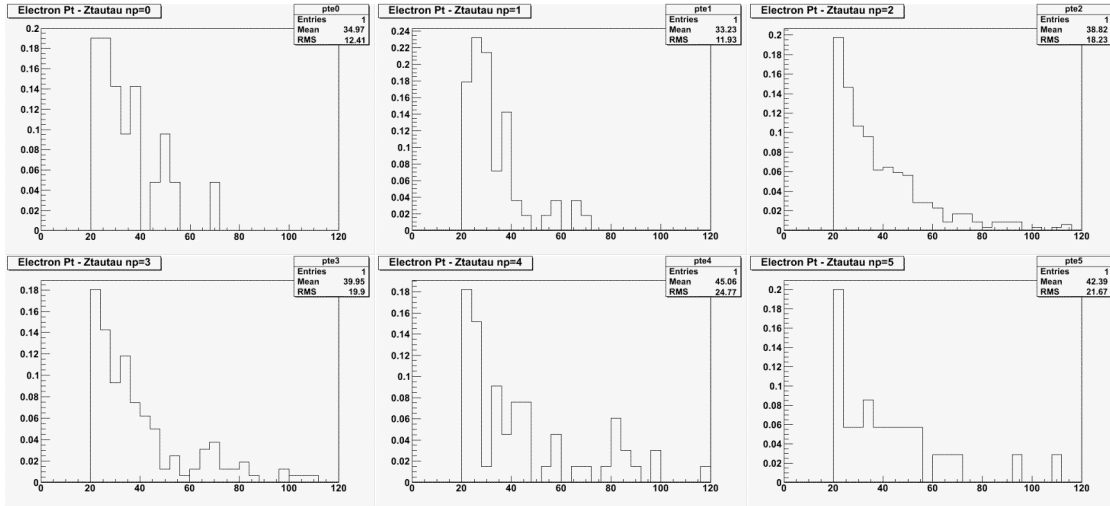


Figure 13 – Electron  $P_T$  distributions.

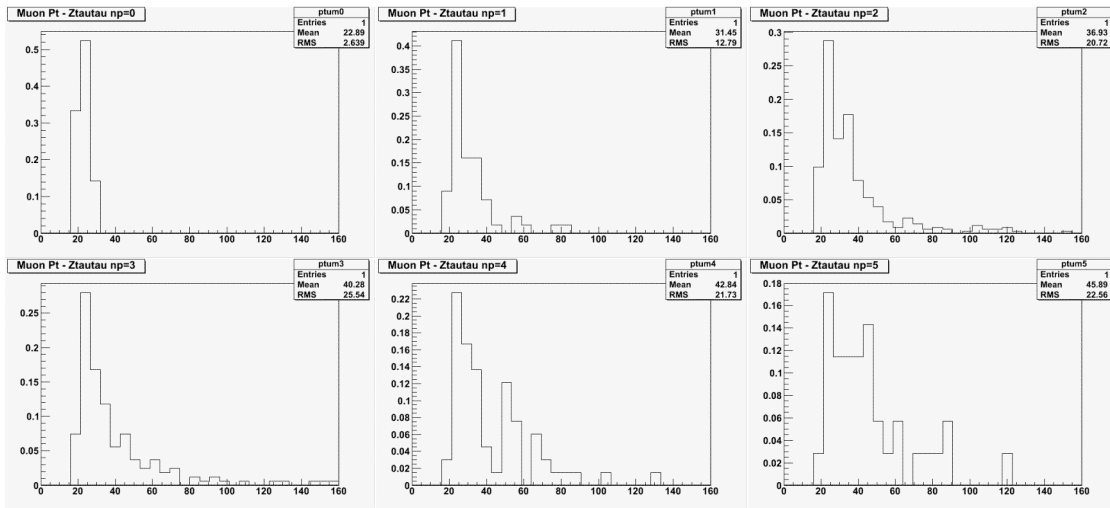


Figure 14 – Muon  $P_T$  distributions.

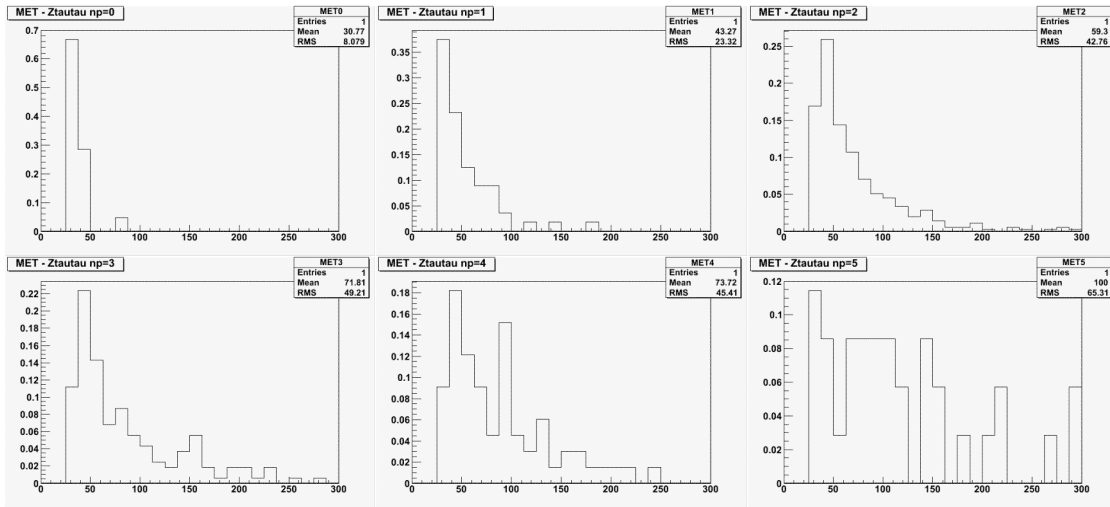


Figure 15 – MET Distributions.

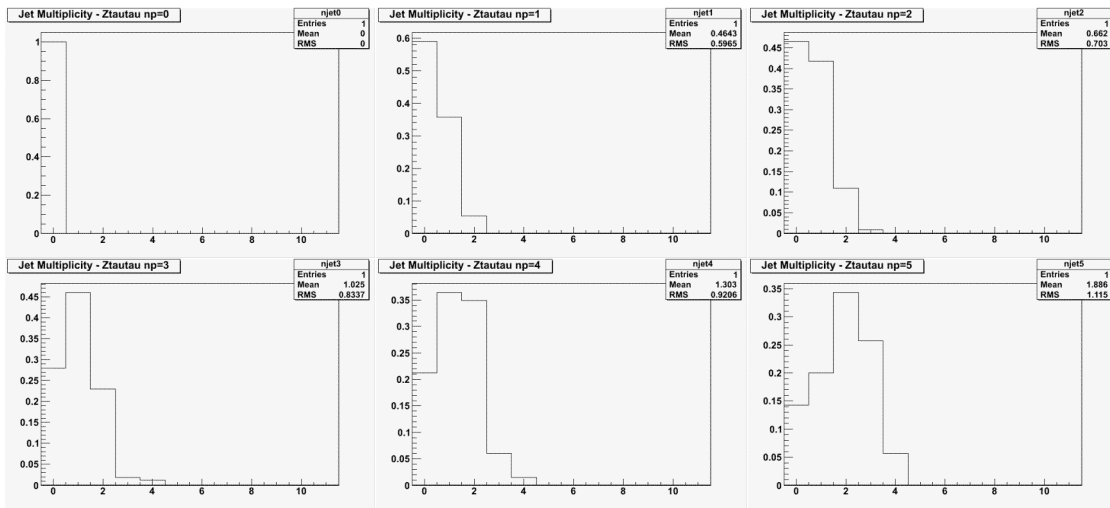


Figure 16 – Jet multiplicity distributions.

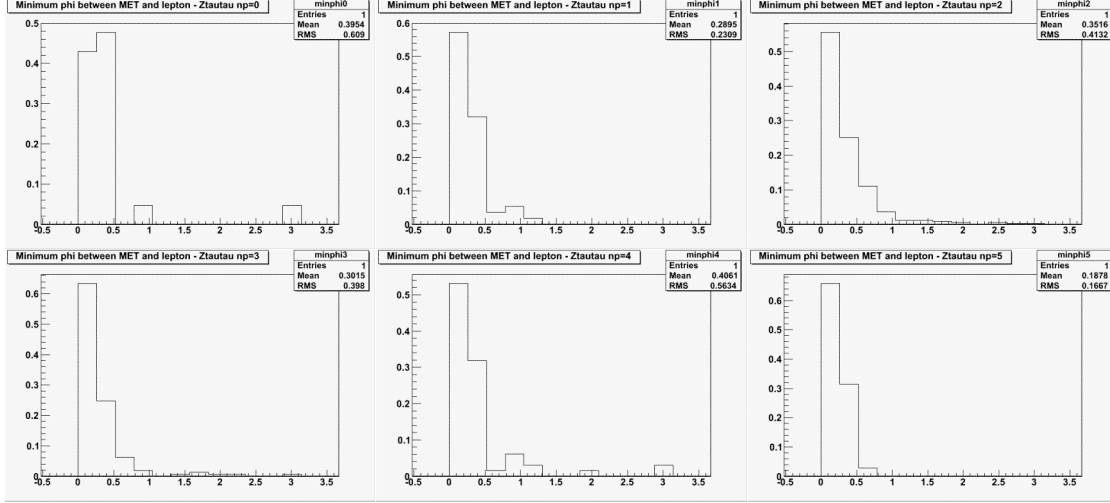


Figure 17 -  $\Delta\phi$  between MET and the nearest lepton.

It appears that as the number of partons increases, the number of jets increases, as we would expect. The other distributions appear to broaden, as a result of the system recoiling against jet activity. Conservation of momentum requires that the vector momentum of the additional jets be cancelled by additional momentum carried by the other particles in the system. The statistics for some of the samples are very low as a result of the cut system (high lepton  $P_T$ , high MET) imposed on them.

## Event Counting and Normalization

Table 4 summarizes the kinematic parameters described above.

		e $\mu$ events $P_t > 20$ GeV	Require oppositely charged leptons	MET > 25 GeV	Jet Multiplicity					
					0	1	2	3	4	5+
t-tbar		3830	3340	2970	774	1160	724	240	60	13
$Z \rightarrow \tau\tau$		2720	2510	413	258	152	59	5	1	0
# of partons	0	1700	1600	70	70	0	0	0	0	0
	1	593	553	188	111	67	10	0	0	0
	2	274	231	119	55	50	13	1	0	0
	3	105	85	53	15	25	12	1	0	0
	4	35	29	21	5	8	7	1	0	0
	5	15	13	11	2	2	4	3	1	0
WW		459	423	320	248	63	9	2	0	0
Wbb		426	192	162	81	71	10	0	0	0

Table 5 – Summary of MC collision dynamics.

The results given are normalized to  $1 \text{ fb}^{-1}$ . In order to properly normalize the samples, the integrated luminosity was calculated from the cross-section and the number of events in each sample. A scaling factor was then applied to bring the luminosity to  $1 \text{ fb}^{-1}$ . A summary of the statistics used in this procedure is given in Table 6.

	Events Generated	GenFilter Efficiency	$\sigma$ (pb)	Integrated Luminosity (fb <sup>-1</sup> )	Scale Factor
t-tbar	4.49 x 10 <sup>6</sup>	0.55	414	19.7	0.051
WW	1 x 10 <sup>5</sup>	0.3717	74	3.63	
Z→ $\tau\tau$ np = 0	2.71 x 10 <sup>5</sup>	1	1230	0.220	
Z→ $\tau\tau$ np = 1		1	286	0.219	
Z→ $\tau\tau$ np = 2		1	96	2.30	
Z→ $\tau\tau$ np = 3		1	29	2.20	
Z→ $\tau\tau$ np = 4		1	8.2	2.26	
Z→ $\tau\tau$ np = 5		1	2.3	2.37	

Table 6 – Summary of scaling procedure.

## Cut-Based Analysis and Conclusions

The goal of this analysis is to examine how cuts affect the signal-to-background ratio of the processes. We wish to accept as many  $t$ - $\bar{t}$  events as possible while rejecting background events. A system of cuts was devised to achieve this: an MET cut, primarily to reduce  $Z \rightarrow \tau\tau$ ; a jet multiplicity cut, to reduce  $Z \rightarrow \tau\tau$ , WW, and W+jets; and a  $\Delta\phi$  cut, primarily to reduce  $Z \rightarrow \tau\tau$ . The statistics associated with these cuts are given in Table 7.

	MET > 25 GeV	Individual Cuts		Both Cuts	Acceptance
		$\Delta\phi$ b/w MET and lepton > 0.5	1+ jets		
$t$ - $\bar{t}$	2970	2320	2197	1720	57.9%
WW	320	284	74	60	18.8%
$Z \rightarrow \tau\tau$	413	72	217	33	8.0%
Wbb	162	152	81	81	50%

Table 7 – Cut statistics.

This simple preliminary sequence of requirements does a reasonable job in preserving most of the top quark signal, while significantly reducing the main backgrounds due to WW and  $Z \rightarrow \tau\tau$ . More study will be needed to further reduce the W + jets contribution. By increasing the ratio of top signal to backgrounds a purer sample of top events can be made available for measuring top properties.

## References

- [1] Griffiths, David. *Introduction to Elementary Particles*. 2<sup>nd</sup> Edition. Wiley-VCH, 2008.
- [2] C Amsler, et al. *Physics Letters, B667(1), 2008*.
- [3] Kruse, Mark. “Observation of Top Quark Pair Production in the Dilepton Decay Channel From Proton-Antiproton Collision at  $\sqrt{s} = 1.8$  TeV.” Doctoral Thesis: Purdue University, 1996.
- [4] European Center for Nuclear Research. <<http://public.web.cern.ch/>>
- [5] Atlas Experiment. <<http://www.atlas.ch/>>
- [6] Kruse, Mark. “The ATLAS Experiment at the LHC.” Talk given 13 November, 2009.